INCOSE PUBLICATIONS

WESTERN STATES REGIONAL CONFERENCE

Systems Engineering Approach to Mitigate Effects of Atmospheric Turbulence for Terrestrial Horizontal Path Imaging Sensors

INCOSE WSRC · 2025

AUTHORS

John Hall, and Steven J. Simske

PUBLICATION DATE

July, 2026

SUBMISSION #

9

SYSTEM ENGINEERING APPROACH TO MITIGATE EFFECTS OF ATMOSPHERIC TURBULENCE FOR TERRESTRIAL HORIZONTAL PATH IMAGING SENSORS

John Hall
Colorado State University
900 Oval Drive
Fort Collins, CO 80523
argyle@colostate.edu

Steven Simske
Colorado State University
900 Oval Drive
Fort Collins, CO 80523
steve.simske@colostate.edu

Abstract

A system engineering process is described for the development of a novel approach toward mitigating the image degrading effects of optical turbulence in a horizontal atmospheric path. The work concentrates on the early phases of the system engineering process involving advanced modeling and ray-tracing. The critical output products are a detailed system concept specification and an associated feasibility analysis which verifies that the approach is both physically possible and economically achievable. A new optical ray-trace analytical method is disclosed which enables development and performance analysis of the system concept.

Keywords

Atmospheric turbulence, aberration, optics, opto-mechanical, infrared, detector, Johnson Criteria, video processing, system architecture.

1.0 Introduction

Strong turbulence within the Earth's atmosphere creates optical aberrations which degrade the image quality of electro-optical imaging sensor systems [1]. Turbulence mitigation for electro-optic sensors working along the horizontal path through the atmosphere has been an ongoing problem for decades [2], and to this day remains a major challenge especially when high image quality is required in "real time", which hereafter is defined as having a maximum lag time of 33 msec between an event in the real scene versus the same event as displayed by the system to a human operator. Attempts to mitigate the turbulence effects have met with limited success, especially in regard to the application of skyward-looking astronomical "adaptive optics" techniques which have not proven successful for terrestrial path applications, and likely never will as discussed by Gronau [3]. When series of consecutive images are collected over time, a technique often referred to as "Lucky Patch" imaging [4] has some proven success, but this approach cannot provide "real time" operation because of its inherent temporal nature. None of the past approaches solve the problem of real-time turbulence mitigation for long-range horizontal path sensors. A system engineering approach can lead to new insight into the nature of the problem and then to a new sensor architecture designed specifically for turbulence mitigation.

1.1 System Engineering Process

The discipline of system engineering has evolved over time, just as machines and devices themselves have become more complicated and now involve greater numbers of scientific disciplines and areas of expertise. The following is a working definition of an "engineered system" in this context: An engineered system is a complex set of interactive components assembled and working together toward one or more common functions. The integration between different engineered systems, the "system of systems", adds further interoperability and complexity. In such cases, broader goals such as sustainability, safety, cyber-security, resilience, and responsiveness are now part of the design process and require more sophisticated overall approaches. There are a variety of system process descriptions available in the literature, and most of them involve three major phases of the life-cycle, namely Concept Development, Engineering Development, and Post-Development [5]. Each stage involves an iterative process of defining requirements and functions, creating designs, and then validating correctness of the designs. The first major step within Concept Development is to elicit the operational goals of the new system. The following list below outlines a representative set of user performance requirements relevant to a sensor which may be adversely impacted by atmospheric turbulence:

REQ.1 System shall be an electro-optical video imaging sensor for use with human observer.

REQ.2 Shall have ability to identify a commercial truck target at a range of at least 2.5 kilometers, including during turbulence atmospheres.

REQ.3 Shall provide performance via passive operation (i.e., no light sources) both night and day.

REQ.4 No noticeable time lag between the real scene and the sensor's output image.

REQ.5 Shall provide HDMI video outputs, command & control via 1553 bus, and keyed connectors.

REQ.6 System shall be compatible with a one-person lift to be lifted onto a tripod and operate along with a pan/tilt mechanism.

REQ.7 System shall run on 24V DC supplied power, maximum current draw 60 amps.

REQ.8 Shall provide engineering diagnostics mode of operation with an expected life before any major repairs are needed for at least two years.

The user performance requirements are the primary input to the Concept Development phase. The design activity can now begin to visualize a system architecture which might be successful. A mathematical model of the system performance is an excellent way to begin the conceptualization, as will be discussed in the following section. The emphasis will encompass requirements 2, 3, and 4 hereafter.

2.0 Imaging System Model

An imaging system model can be instructed which includes all interacting elements, both natural and engineered. to include the target, atmosphere, illumination, optics, detector, image processor, output display, and the human operator. From a mathematical point of view, each of these block segments will have its own set of responses to inputs, as well as its own form of output or "transfer function" which feeds into the next block in sequence. Figure 2.0-1 below shows a suitable block diagram for an electro-optical imaging sensor [6,7].

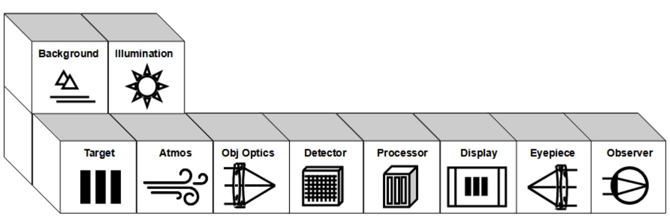

Figure 2.0-1: Block Diagram for Electro-Optical Sensor Performance Model

The target is a physical object, which from a mathematical linear system point of view is comprised of the superposition of a number of point sources, each emitting a measure of optical light within the spectrum of concern [6]. The emitted light which is captured by the sensor system constitutes the "signal" from each object point. This signal is known to also contain a predictable amount of Poisson noise due to random, non-linear photon interactions [6]. The target optical emission signal must be contrasted against the emissions from surrounding background objects in order for a human to "see" the target. It is immediately recognized from the objectives that a visible spectrum sensor will struggle with night operations, and thus an infrared imager is the best general approach as will be briefly shown here. For a ground-based infrared imager, it is reasonable to assume the source of the photon flux in natural environments is mostly from blackbody radiation [7]. Max Planck demonstrated that the emission spectrum of a blackbody object will obey an exponential equation which is a function of a set of constants, the object temperature (T), and the specific wavelength in question (λ). The formulation for blackbody emittance B(T) in units of Watts/m^2/sr/micron is then given per the following [8]:

$$B(T) = [2hc^2/\lambda^5] \div [\exp(hc/\lambda kT) - 1] \qquad (1)$$

with the Plank constant $h = 6.63 \times 10^{-34}$ Joule-seconds, the Boltzmann constant is $k = 1.38 \times 10^{-23}$ Joules/Kelvin, and the speed of light c = 299,792,458 meters/second.

2.1 Atmospheric Effects

The optical signal from the target propagates through the atmosphere and may encounter absorption and optical ray path distortions as a function of the weather conditions and turbulence magnitude which is characterized by the atmospheric structure parameter (C_n^2)[9]. Turbulence varies with the viewing angle relative to the sensor's optics. In optical terms, this means that if the angular separation between the points is large enough, the aberration coefficients for any point within the sensor field of view may be uncorrelated to those of another point. Close neighboring field points, however, may have the same basic turbulence structure and can be imagined as a "patch" within the larger field. The optical aberrations of all points within a patch are strongly correlated, and thus the term "isoplanatic" is used to describe the consistent optical behavior within the patch area. The maximum isoplanatic field angle θ_0, typically given in units of μrad, over which the optical wavefront can be assumed to be constant, and is given by the following equation [10]:

$$\theta_0 = [\ 2.91 \cdot (2\pi/\lambda)^2 \cdot (L)^{2.667} \cdot (3/8) \ \cdot (C_n^{\ 2})]\ ]^{-0.6} \qquad (2)$$

Figure 2.1-1 below illustrates a ground sensor field of view which typically will contain many isoplanatic patches. This is an extremely important consideration for sensor concept development, for as Gronau had demonstrated [3], an astronomical approach utilizing adaptive optics techniques is capable of correcting only one patch at a time and thus will be unacceptable for real-time horizontal path imaging for a typical ground sensor application.

Figure 2.1-1: Conceptual Distribution of Multiple Isoplanatic Patches Across the Field of View.

The intensities and distributions of atmospheric turbulence effects will vary as a function of time. Fried discusses the fact that the temporal rate of random fluctuation can have an effect on an imaging system, depending on the integration time (τ) of the sensor's detector. The temporal rate of change is related to the Fried Parameter (r_0) and the average wind velocity (v_{av}) as follows [1]:

$$t_0 = r_0 \div v_{av} \qquad (3)$$

where v_{av} has units of m/sec and t_0 has units of msec. Avoidance of motion-induced blur due to turbulence variations thus requires that $\tau < t_0$ on average. Table 2.1-A below shows a span of typical turbulence parameters for the infrared spectrum at a fixed range of 3.0 km.

Table 2.1-A: Example of Atmospheric Turbulence Range-Dependent Parameters

INPUT				CALCULATION		
λ (μm)	L (Km)	$C_n^{\ 2}$ ($m^{-0.667}$)	v_{av} (m/sec)	r_0 (mm)	θ_0 (μrad)	t_0 (msec)
10	3	1.00E-15	10.00	2727.16	285.78	272.72
10	3	5.00E-15	10.00	1038.31	108.81	103.83
10	3	1.00E-14	10.00	685.03	71.79	68.50
10	3	5.00E-14	10.00	260.81	27.33	26.08
10	3	1.00E-13	10.00	172.07	18.03	17.21
10	3	5.00E-13	10.00	65.51	6.87	6.55
10	3	1.00E-12	10.00	43.22	4.53	4.32

2.2 Composite Modulation Transfer Function

The "system" as an engineered device begins with the objective optics. The objective lens receives a portion of the target's optical emittance and focuses that light on a point-by-point basis into a real image onto the photo-detector [11]. The detector is comprised of materials which convert the incoming light radiation into a corresponding electrical signal. Typically, there is a range of intensity values over which the output is linear versus the input. However, if the input is either too low or too high, then a non-linear response may be output. The electrical signal is amplified and eventually converted into a digital output signal. The digital signal is then operated upon by processor electronics which can provide various calibrations, noise abatement, and conditioning for the display block which follows. The display may be a conventional computer monitor which is directly viewed, or it may be a smaller screen which is viewed through a magnifying eyepiece. Finally, the human eye receives the image which is then to be processed by the human brain. The linear responses of the entire system including turbulence can be characterized by the System Modulation Transfer Function (MTF_{sys}), which is in turn the product of individual MTF components as follows [6, 7]:

$$MTF_{sys}(\xi) = MTF_{tur}(\xi) \cdot MTF_{opt}(\xi) \cdot MTF_{\beta}(\xi) \cdot MTF_{pix}(\xi) \cdot MTF_{jit}(\xi) \cdot MTF_{\varphi}(\xi) \qquad (4)$$

Individual component MTF's are formulated as follows:

$$MTF_{tur}(\xi) = \exp[(-57.4) \cdot (3/8) \cdot (\xi)^{1.667} \cdot (C_n^2) \cdot (\lambda)^{-0.333} \cdot L \cdot (1 - 0.5(\lambda\xi/D)^{0.333})] \qquad (4a)$$

$$MTF_{opt}(\xi) = (2/\pi) \cdot [\eta - \cos(\eta)\sin(\eta)]; \text{ where } \eta = \cos^{-1}(\lambda \cdot \xi \cdot F\#) \qquad (4b)$$

$$MTF_{\beta} = \mathrm{sinc}[(8 \cdot \xi \cdot \beta_{010} \cdot F\#)(1 - (\xi \cdot \lambda \cdot F\#))] \qquad (4c)$$

$$MTF_{pix}(\xi) = [\sin(2\pi \cdot \omega \cdot \xi)] \div [2\pi \cdot \omega \cdot \xi] = \mathrm{sinc}(2\pi \cdot \omega \cdot \xi) \qquad 4(d)$$

$$MTF_{\varphi}(\psi) = \exp[-2(\pi\varphi\psi)^2] \qquad 4(e)$$

$$MTF_{jit} = \exp[-2(\pi\, \sigma_{jit}\, \xi)^2] \qquad 4(f)$$

where ξ is the variable spatial frequency in cycles/mrad and the other variables are per the following Table 2.2-A of example values:

Table 2.2-A: Model Input Values

Variable	Description	Value	Units
d_{ζ}	Target critical dimension	2.3	meters
λ_1	Spectral band, lower limit	7.5	µm
λ_2	Spectral band, upper limit	12.0	µm
ΔT	Target-to-background temperature difference	1.25	K
T	Average Background Temperature	300	K
a	Atm. Absorption coefficient (70% per km)	0.356	km^{-1}
C_n^2	Atmospheric Index Structure (mild turbulence)	1×10^{-15}	$m^{-0.667}$
f	Objective Lens focal length	400	mm
F#	Objective Lens F#	3	(no unit)
Υ_{β}	Objective Lens total transmission	0.70	(%)
β_{010}	Objective Lens Defocus aberration	0.25	waves (λ_m)
ω	Detector Element Pitch (square sides)	0.028	mm
W	Detector well capacity maximum	12M	e^-
QE	Detector Quantum Efficiency	0.80	(%)
τ	Detector integration time	7×10^{-5}	sec
σ_e	Detector & Electronics total RMS noise	1200	e^-
σ_{jit}	Stabilization/jitter RMS	.005	mrad
φ	Display Blur RMS	0.145	mrad
M	System Magnification	9.5	(scalar)
$\mathfrak{h}_i$	Johnson Cycle Criteria for Identification	6.4	cycles

The results of the system MTF model are shown below in Figure 2.2-1 for cases of both low turbulence and high turbulence conditions. The dashed line shows the MTF impact specifically for the range-dependent turbulence component, which becomes the dominant contributor as the C_n^2 value moves from an initial 1.0×10^{-15} to a more severe value of 5.0×10^{-13} $m^{-0.667}$. Since all other parameters are unchanged, this analysis shows the impact of atmospheric turbulence across a range of reasonable values. It also confirms that some form of mitigation will be needed to mitigate the loss in range performance.

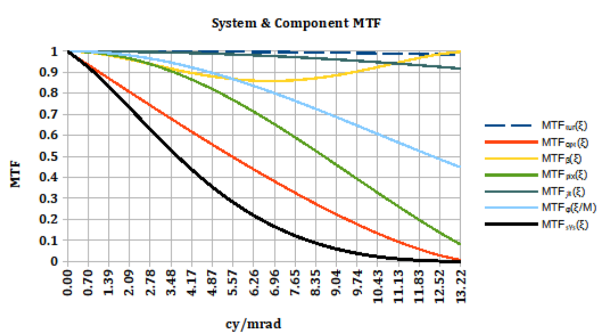

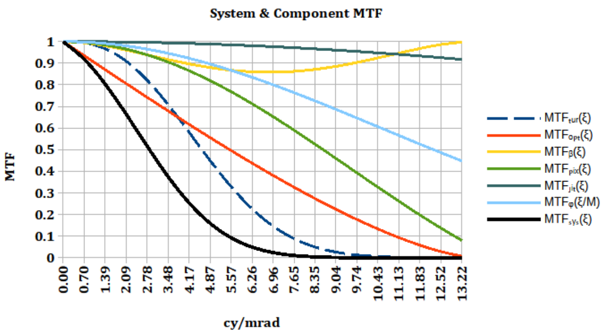

Figure 2.2-1: Plots of Linear Response Component & System MTF for Low Turbulence (upper, $C_n^2 = 1.0 \times 10^{-15}$) and High Turbulence (lower, $C_n^2 = 5.0 \times 10^{-13}$)

2.3 Non-Linear Limits to MTF Model

As the MTF reaches lower values, eventually the amount of contrast becomes lost in the non-linear noise of the system. This noise can often be assumed to be dominated by photon noise, but electrical noise and other independent factors if known can be included via a root-sum-square (RSS) calculation to find the system-level signal-to-noise ratio (SNR). The temperature difference between target and background where the signal contrast is exactly equal to the noise is referred to as the noise equivalent delta-T, or "NEΔT" value [7]. An example calculation for sensor noise parameters is shown in the Table 2.3-A below using the parameters from Table 2.2-A earlier, resulting in a NEΔT = 27 mK which is within the capability of many commercially available infrared detectors [13]:

Table 2.3-A: Sensor Noise Calculations

Backgrnd T	Target T	λ_1	λ_m	λ_2	F#	P (w_{Pix})	Υ_β	τ	QE	Max Well	σ_e
K	K	µm	µm	µm	(-)	mm	%	sec	%	e^-	e^-
300.000	300.027	7.5	9.75	12	3	0.028	0.7	7.00E-05	0.85	1.20E+07	1200
Backgrnd e^-	Target e^-	Well Fill	Δe^-	σ_p	σ_{rms}	SNR	ΔT				
5.9953E+06	5.9980E+06	50%	2,719	2,449	2,727	1.00	0.027				

Once the sensor noise parameters are known, they can be incorporated into the system model as a "load line" beyond which the MTF predictions are no longer valid [7]. These noise effect parameters such as atmospheric attenuation or turbulence degradation are functions of the range between sensor and target, and so a mathematical treatment is needed to account for range dependencies. The Johnson Criteria (J_i) provides a means by which the cy/mrad scale of the sensor MTF can be converted to target range, typically in kilometers (km), for a specific cognitive function of detection, recognition, or identification [12]. The crossover point where the MTF meets the non-linear noise "load line" is the range up to which the system has a linear and thus predictable response. It is common practice to specify system performance in multiple weather conditions and cognitive tasks, each case thus having its own unique load line crossing the system MTF typically at a different point, but only one load line is demonstrated here. The figures below show the systems models for the parameters in Table 2.2-2 with both low and high turbulence.

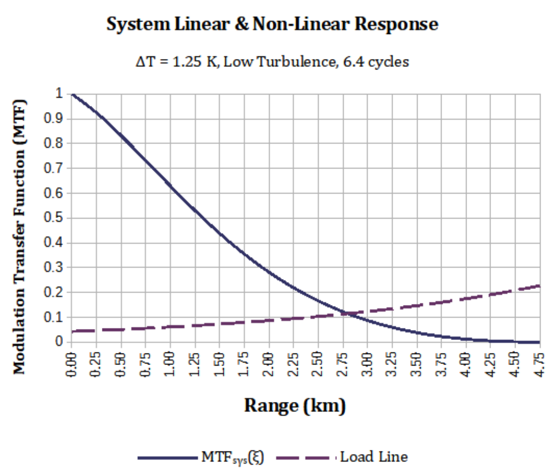

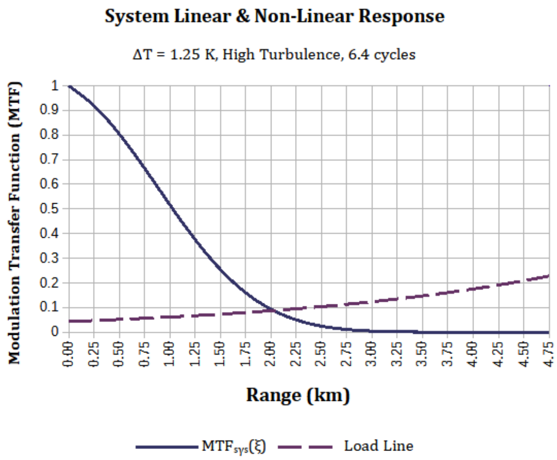

Figure 2.2-2: Sensor Maximum Range Occurs at Crossover Between Linear & Non-Linear Regions for Low & High Turbulence Cases

3.0 NOVEL OPTICAL RAY-TRACE ANALYSIS

The system performance model can estimate the mean impact to the system MTF based on the turbulence strength but unfortunately does not provide much detail about what is actually occurring at individual image points within the field. There have been successful mathematical models of individual isoplanatic image segments [14], and real-time simulations have been proposed [2], but none of the prior art integrates into a complete optical model of both the Atmosphere and the Objective Optics over a wide field of view. This is a significant gap area between the researchers and the system designers. A method of ray-tracing through special surfaces is offered here as a means of modeling a turbulent atmosphere as if it were a component within the Objective Lens optical system. The lens model technique can be implemented in commercial lens design software packages such as Zemax, CODE V, or the venerable ACCOS V of which an open-source version, KDP, is used herein. A turbulence-simulation phaseplate is added to the lens and placed very near to the focal plane. The phaseplate contains a surface sag function which causes different parts of the field of view to experience different amounts of optical aberration, thus providing a means to approximate the effects of multiple isoplanatic patches occurring within the sensor's field of view as shown in the Figure 3.0-1 below for a simple infrared imaging singlet made of Germanium material and having a 69.43 mm focal length, a total field angle of 7.0°, and an aperture diameter of 20.0 mm. The phaseplate substrate material is ZnSe with 1.0 mm thickness and located 0.787 mm in front of the nominal focal plane.

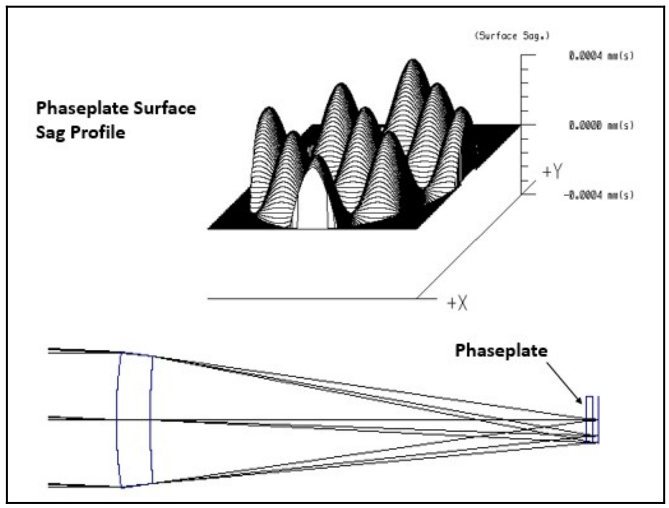

Figure 3.0-1: Image Forming Optical System with Phaseplate Turbulence Simulator Near Focal Plane of an Imaging Lens (Profile Exaggerated Scale for Clarity)

The surface sag z for the phaseplate is given by the following equation, which adds two crossed sinusoidal waves to a basic lens curvature:

$$z = [(cr^2) \div [1 + (1 - (1 + k)c^2r^2)^{0.5}]] - A[(\tfrac{1}{4})[1 + \cos(2\pi\alpha x)][1 + \cos(2\pi\beta y)] - 1] \quad (5)$$

The equation includes the conventional lens parameters for curvature c, the radial coordinate r within the aperture, and the conic constant k for parabolic or hyperbolic shapes. The scale parameter A is the peak-to-valley (PV) height in lens units (mm) of the cosine modulation terms. In this example, the PV amplitude is set to 0.10 mm, which is ten times the wavelength, to simulate a severe turbulence aberration. The values α and β are the spatial periods of the cosine oscillations in the x and y directions, respectively, in units of length (mm). The periods shown in the example are both set to 2.0 mm, which yields roughly four sinusoidal cycles across the 8.46 mm image format height. Small period values create phase patterns which change as a function of field angle, whereas large periods induce nearly the same phase change over many or all field points simultaneously. This enables the model to account for turbulence down range, which can change radically with field angle, as well as turbulence immediately in front of the sensor aperture which has little field angle dependence. The ability to model the effects of a turbulent medium on the optical ray paths across a larger field of view provides a greater intuitive visualization of the problem, and it provides a new tool with which a candidate system design approach can be evaluated and validated. In the example Figure 3.0-2 below, the positions of the rays for non-turbulence and turbulence cases can be quickly compared. It is notable that image defocus is strongly correlated to individual positions within the field of view. Indeed, the new ray-trace method reveals intuitively that a multi-focal capture system could in theory locate the "lucky" points of the turbulated image as a function of defocus and field position.

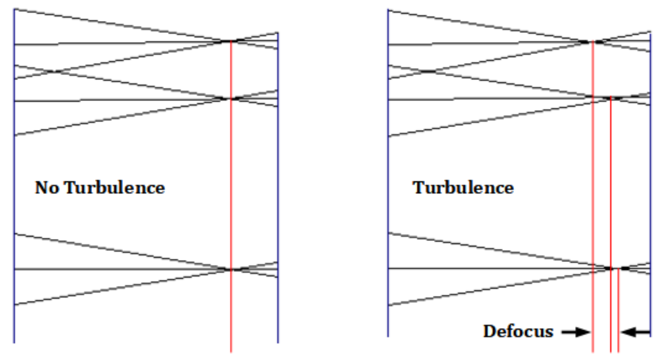

Figure 3.0-2: Ray Trace Model Shows Field-Dependent Defocus Effects of Turbulence

The ray-trace model can also be used to answer a critical question, “If we could design a system with multi-focal capture, how much of the turbulence aberration might be removed?” Table 3.0-A below shows the values for the defocused PSF for the on-axis field, where "PV" refers to the peak-to-valley error at 10 µm wavelength and "RMS WFE" is the root-mean-square wavefront error value. The RMS WFE is an averaged value over all traced rays, so it is typically less than the PV which is the absolute value of the worst-case error for any single ray. The first two columns where Δz = 0 show the impact of the turbulence, which is about a 0.15 ÷ 0.036 = 417% increase (i.e., a degradation) in RMS WFE at the nominal focal plane position. At the defocus position of Δz = 0.4 mm, however, that degradation is reduced by about 2X which is a substantial improvement.

Table 3.0-A: Variation of WFE vs. Defocus Position

	no turbulence	turbulence	defocus (1)	defocus (2)	defocus (3)
Δz	0.0	0.0	0.2	0.4	0.6
PV	0.21	0.56	0.33	0.37	0.60
RMS WFE	0.036	0.15	0.07	0.06	0.14

The ray trace model indicates that a multi-focal capture system has great potential to reduce the adverse effects of atmospheric turbulence by factors of 2X or more. The next question now becomes, “How can a system architecture be conceived which performs the multi-focal capture and imaging processing for real-time image display?”

4.0 SYSTEM SYNTHESIS

A system architecture can now be conceived based on capturing several planes of defocus within the time allowed by the turbulence temporal rage of change (t_0). The key aspects of the system begin with an opto-mechanical method of rapidly capturing planes of defocus and then proceed with an algorithm which selects the pixels with the highest contrast ratios across each focal plane from which an optimized two-dimensional image frame is output. There has been some recent research published in this area [15], but the system architecture and algorithm calculation must be quick such that lag time is minimized for "real time" usage in the field. Furthermore, the rapidity of the defocus capture needs to be balanced against the signal-to-noise ratio (SNR) capability of the sensor such that the contrast resolution of the displayed imagery is good enough for the human operator to perform the desired visual tasks.

4.1 Opto-Mechanical Approach

One possible opto-mechanical architecture for rapid image forming utilizes a linear scanned infrared detector array as shown in Figure 4.1-1 below. One-dimensional motion of the scan mirror pans the projection of the linear pixel array across the horizontal field, thereby capturing a two-dimensional image over a scan time period.

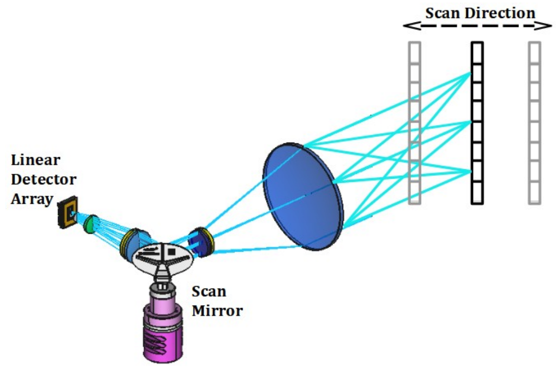

Figure 4.1-1: Linear Scanned Array System Opto-Mechanical Architecture

A small number of detector columns can be set in tandem where each column corresponds to one of the defocus positions. Indeed, a parallel column architecture such as 240 × 4 rows and columns of pixels can be used for a technique called "time delayed integration" to boost the signal-to-noise ratio (SNR) [7], but for turbulence mitigation these same parallel columns may instead each be assigned a specific defocus value. Optical prisms can be used to induce the defocus effect spanning across each linear column. Figure 4.1-2 below shows an example of a 1 mm center-line thickness prism made from Germanium material (n = 4.0) and with a 5° physical tilt on the first surface relative to the optical axis.

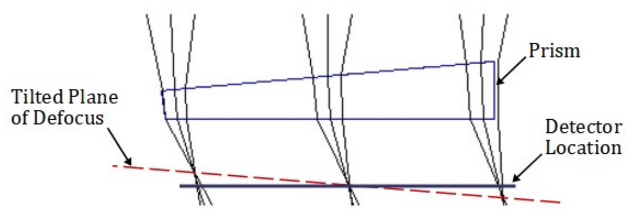

Figure 4.1-2: Prism Induced Defocus in the Scan Direction

4.2 Algorithm

A digital algorithm can be used to choose the best focus position on a pixel-by-pixel basis [16]. For example, a simple and parsimonious algorithm can calculate the edge gradients of the same pixel location in each of the five planes of focus. For any pixel intensity value P(n,m) as a function of n rows and m columns in a single plane of defocus, the edge gradient score (EDG) can be defined per the following:

$$EDG(P) = 4P(n,m) - P(n+1,m) - P(n-1,m) - P(n,m-1) - P(n,m+1) \quad (6)$$

The maximum edge score pixel among the defocus planes becomes the output value for the image video frame. The algorithm does not require convolution operations and hence can be done almost as quickly as the pixel values are captured by the video process chain. The optical ray analysis predicts the result and allows the performance model parameters to be adjusted. The ray-trace showed the PSF was improved by roughly a factor of 2X, thus it is reasonable to estimate that the MTF cutoff frequency of the turbulence component can likewise be improved by roughly a factor of two. In the original model for high turbulence conditions where $C_n^2 = 5.05 \times 10^{-13}$, the $MTF_{tur}(\xi)$ component reached near zero contrast at about 10 cy/mrad. Therefore, decreasing the PSF by two would extend the cutoff to nearly 20 cy/mrad. This can be realized in the model with trial and error by finding an equivalent index structure parameter of about $C_n^2 = 1.00 \times 10^{-13}$ which approximates the corrected MTF. This change increases the sensor targeting range to 2.5 km as shown below in Figure 4.2-1. This is a significant increase. Further all-digital image processing techniques might be able to further improve the output image quality [17].

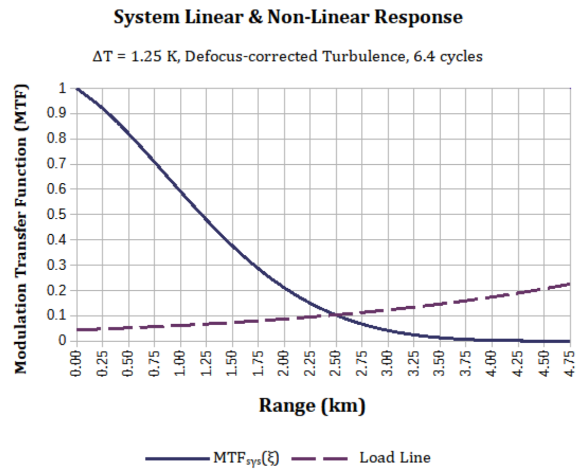

Figure 4.2-1: Predicted Improved System Range Via Multi-Focal Image Processing

4.3 Feasible System Architecture

The system architecture concept can be comprised of several mature technologies, including linear infrared focal plane detector arrays [13] as previously discussed. Certain components such as the imaging optics and defocus prisms may be customized according to specific customer objectives, but design forms and materials are mature and readily available [18]. Galvanic scanning mechanisms [19] and cryogenic cooling subsystems [20, 21] are well known in the art and commercially available [22]. Video processor "system-on-chip" (SOC) devices are available in the commercial markets. The following figure shows a mechanical model visualization of the critical system components. The physical model, along with information from various product data sheets, provides confidence at this initial stage that specifications such as one-person carry, total system power, and Mean Time Between Failure (MTBF) can also be met.

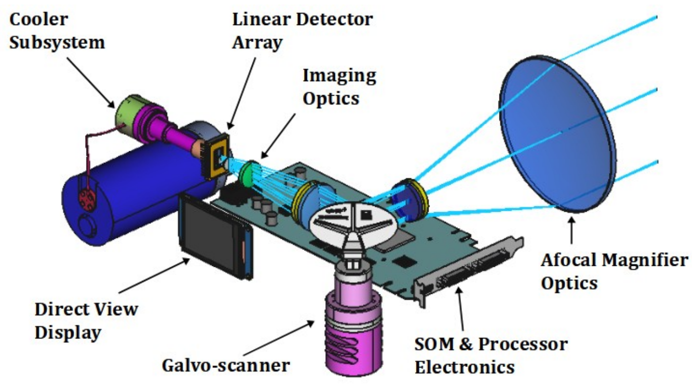

Figure 4.3-1: Visualization of System Critical Components

The system electronics estimate is based on the commercial GeForce GTX 560 video processor, whose power consumption is rated at about 150 W. For the display, the Displaytech DT028BTFT liquid crystal display panel is referenced as an "as-like" component. Its operating current is reported to be 80 mA at an input voltage of 3V, resulting in a total power draw of 0.240 W. The sum of these component estimates provides a sound basis for the initial budget estimate. In some cases, it is also necessary to assign an upper range limit to account for issues such as exterior environmental temperatures or power-on surges. Both nominal and surge/limit cases are provided in the initial system power budget per Table 4.3-A below which has significant margin over the user requirement of operating at 12V and maximum 60 amps, resulting maximum allowed power of 1440 W.

Table 4.3-A: Initial Power Budget

Component	Nominal (W)	Surge/Limit (W)
Scanner	25.0	60.0
Detector	1.0	1.0
Cooler	35.0	70.0
Electronics	100.0	150.0
Display	0.50	0.50
TOTAL (W)	161.5	281.50

The "one-person lift" user requirement is the critical metric for the system weight allocation. The applicable standard for this parameter is found in MIL-STD-1472F [24], para. 5.9.11.3.5, Table XVII, for handling function A, male and female population. The requirement for a one-person carry is thus 37 lbs. maximum item weight. The detailed system design does not yet exist, and so an initial budget estimate is obtained from internally generated CAD models and available commercial data for similar parts and components. Table 4.3-B below shows the results. There is almost no margin in this initial estimate versus the requirement. The system weight is thus flagged for weight reduction activities during the detailed design process and might require a special oversight team to monitor the design process closely. The "big hitters" for weight are the interior bench and outer chassis mechanical parts, and the challenge will be to reduce total mass while at the same time providing structural rigidity and vibration isolation.

Table 4.3-B: Initial Weight Budget

Component	Data Source	Weight (lbs)
IR Optics	Optical ray-trace CAD model	1.25
Scanner Module	ThorLabs QS45X-AG	3.0
Cooler Package	Cobham LC1065 data sheet	2.5
Focal Plane Detector	ref. King, based on 4 lb IDECA	1.5
Display Panel	DisplayTech DT028BTFT	.25
Processor electronics	GeForce GTX 560	1.75
Inner bench structure	CAD estimate, aluminum	8.75
Outer chassis	Hoffman A16H1608AALP aluminum enclosure	14.0
Misc. parts & cables	Engineering Estimate	3.5
TOTAL		**36.5**

The Reliability analysis is essential to support the product warranty which defines the responsibility of the original equipment manufacturer (OEM) in the event that the system for some reason fails to operate properly. The procedures for establishing reliability estimates are explained thoroughly in MIL-STD-781, published by the US Department of Defense [25]. Revision C of this document is particularly useful because it contains details of the mathematics involved. The engineering reliability budget begins by first collecting the Mean Time Between Failure (MTBF) of the subsystems and components. MTBF data given in units of hours, or its reciprocal failure rate per million hours (Λ), is often available from the component manufacturers. The conversion between the two, when MTBF is given in hours, is as follows:

$$\Lambda = (\mathrm{MTBF})^{-1} \quad (7)$$

MIL-HDBK-217 [26] also contains sets of data for common electronics components . For example, if a component has a published MTBF value of 250,000 hours then the failure rate is $\Lambda = 4.0 \times 10^{-6}$ failures per hour of operation. The reliability (REL), or "probability of survival" for a given time interval (t), is then an exponential function given by the following equation:

$$\mathrm{REL}(t) = \exp(-\Lambda t) \quad (8)$$

For example, the probability of the system functioning for the time period (t) of one system-level MBTF, i.e., where t = MTBF = Λ^{-1}, solves as REL = exp(-1) = 0.3678, or 36.78%. For the sensor system, the following Table 4.3-C shows an initial high-level reliability budget:

Table 4.3-C: Initial Reliability Budget

Item	MTBF	$\Lambda = (\mathrm{MTBF})^{-1}$
Afocal Optic	200,000	5.00E-06
Image Optic	250,000	4.00E-06
Galvo-scan	100,000	1.00E-05
Detector	60,000	1.67E-05
Cryo-Cooler	40,000	2.50E-05
SOM/elect	400,000	2.50E-06
Display	600,000	1.67E-06

Assuming all the items are used in series with no redundancy, the system-level failure rate is the sum of the individual item rates, i.e.,

$$\Lambda_{sys} = \sum_n \Lambda_n \quad (9)$$

For the above example, $\Lambda_{sys} = 6.48 \times 10^{-5}$ becomes the input value to feed the reliability (REL) calculation for a range of time values (t) in hours. Since the function is exponential, it is helpful to show most of the curve on a log scale ranging from zero to one million hours per the following Figure 4.3-2:

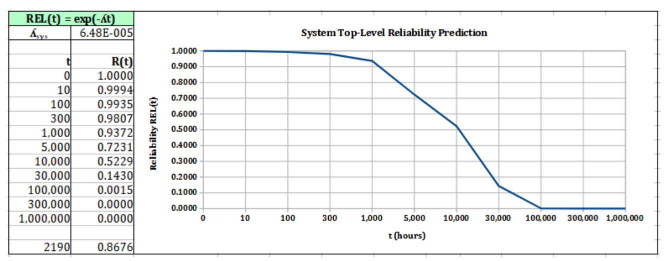

Figure 4.3-2: Initial Reliability Life Prediction

4.4 Compliance Matrix

Table 4.4-A below shows a matrix which identifies which shows traceability of development specifications back to one or more of the original customer objectives. It is common that user objectives are complex and must be decomposed into multiple elemental system specifications, such that each system requirement is singularly "atomic" and measurable [23]. Specifications for

environmental effects and human ergonomics and safety have been added to round out the listing. During advanced development, details of each subsystem and component will result in additional specifications and detailed tolerance ranges which may be added to this initial listing. A key aspect of the specifications is that the multi-focal capture occurs within a "real time" instance, which must balance the varying atmospheric time constants, the detector integration time versus well fill, the scan period, and the video output frame rate. Once the design evolves into final form, additional cross-matrix columns can later be added to group together common quality verification such as the First Article Test, Operational Test, and production Acceptance Test.

Table 4.4-A: Partial Development Specification Traceability Matrix

#	Requirement	Value	Customer Requirement							
			1	*2*	*3*	*4*	*5*	*6*	*7*	*8*
	RANGE MODEL & TURBULENCE PARAMETERS									
1.1	Target Identification Range Minimum	2.5 km	x	x	x					
1.2	Target critical dimension	2.3 meter		x	x					
1.3	Spectral band, lower limit	7.5 micron			x					
1.4	Spectral band, upper limit	12.0 micron			x					
1.5	Target-to-background temperature difference	1.25 K		x	x					
1.6	Average Background Temperature	300 K		x	x					
1.7	Atmos. Absorption coefficient (70% per km)	0.356		x	x					
1.8	Atmospheric Index Structure (low turbulence)	$1 \times 10^{-[illegible]}$		x						
1.9	Atmospheric Index Structure (strong turb)	5×10^{-12}		x						
1.10	Objective Lens focal length	400 mm		x						
1.11	Objective Lens F#	3		x						
1.12	Objective Lens total transmission	0.70		x						
1.13	Objective Lens Maximum Aberration	0.25λ		x						
1.14	Detector Element Pitch (square sides)	0.028 mm		x						
1.15	Detector well capacity maximum	12M		x	x					
1.16	Detector Quantum Efficiency	0.80		x	x					
1.17	Detector integration time	$7 \times 10^{-[illegible]}$ sec		x	x	x				
1.18	Detector & Electronics total RMS noise	1200 e^-		x	x					
1.19	Stabilization/jitter RMS	0.005 mrad		x	x			x		
1.20	Maximum Display Blur RMS	0.145 mrad	x	x	x					
1.21	System Magnification	9.5X	x	x	x					
1.22	Johnson Criteria for Identification	6.4 cycles	x	x	x					
1.23	Focal Capture Defocus Steps (total)	5 steps		x	x					
1.24	Focal Capture Defocus Step Increment	±0.30 mm		x	x					
1.25	Focal Capture Total Time Period Maximum	Single Frame		x	x	x				
1.26	Frame Rate	60 Hz	x	x	x	x	x			
1.27	Total Video Lag Time Maximum	16 msec	x	x	x	x	x			
	PHYSICAL & LIFETIME SPECIFICATIONS									
2.1	Weight/Mass	35.25 lbs						x		
2.2	Size/Volume	18" × 18" × 12"						x		
2.3	Electrical Power Maximum	24v, 60 amp							x	
2.4	Reliability	90% at 1000 hrs			x			x		x

5.0 CONCLUSION

The system engineering method has been used to synthesize a new sensor architecture which is well suited for the task of mitigating the image degradation caused by atmospheric turbulence. A general system performance model is described which includes both linear and non-linear effects. A novel optical ray-trace method permits evaluation of the impacts of turbulence as a function of field angle and provides great insight for possible methods of mitigation such as the capture of multiple planes of defocus within a single frame time period. A feasible sensor configuration for multi-focal capture was outlined using available technologies coupled with algorithms which can conceivably run with minimal time lag. A specification compliance matrix shows how each detail of the system architecture complies with the customer performance objectives, with particular emphasis on meeting user requirements 2, 3, and 4.

Acknowlegement

This work was sponsored by the US Army DEVCOM C5ISR, Fort Belvoir, VA 22060.

References

1. Fried, D., "Optical Resolution Through a Randomly Inhomogeneous Medium for Very Long and Very Short Exposures", J. Opt. Soc. America, Vol. 56, No. 10, October, 1966.
2. Schutte, K., van Eekeren, A., Dijk, J., Schwering, P., van Iersel,M., Doelman N., "An overview of turbulence compensation",

Proceedings of SPIE, Vol. 8542, Electro-Optical Remote Sensing, Photonic Technologies, and Applications VI, ,2012.
3. Gronau, Y., "Limitations of Adaptive Optics for Imaging at Horizontal Paths", Vol. 1968, 1993.
4. Vorontsov, M., Ricklin, J., Miller, W., Irochnikov, N., "Optical simulation of imaging systems using multiple turbulent phase screens", Proc. SPIE, Vol. 2312, Optics in Atmospheric Propagation and Random Phenomena, December, 1994.
5. Kossiakoff, A., Sweet, W., Seymour, S., Biemer, S., Systems Engineering Principles and Practice, 2nd ed., John Wiley & Sons, Inc., Hoboken, NJ, 2011.
6. Lloyd, J. M., Thermal Imaging Systems, Plenum Press, New York, 1975.
7. Driggers, R., Cox, P., Edwards, T., Introduction to Infrared and Electro-Optical Systems, Artech House, Norwood, MA, 1999.
8. Planck, M., "Ueber das Gesetz der Energieverteilung im Normalspectrum", Annalen der Physik, pp. 553-563, March, 1901.
9. Tatarskii, V. I., "The Effects of Turbulent Atmosphere on Wave Propagation", TT 68-50464, National Oceanic & Atmospheric Administration (NOAA),1971.
10. D. Sadot, S. Shamirz, I. Sasson, I. Dror, N. S. Kopeika, “Prediction of Overall Atmospheric Modulation Transfer Function with Standard Weather Parameters: Comparison with Measurements with Two Imaging Systems,” OE, 34(11), 3239-3249 (1995).
11. O'Neill, E. L., *Introduction to Statistical Optics*, Addison-Wesley, Reading, MA, 1963.
12. Johnson, J., "Analysis of Image Forming Systems", US Army Engineering Research & Development Laboratories, Proceedings of the Image Intensifier Symposium, 1958.
13. Filachev, A., Ponomarenko, V., Taubkin, I., Ushakova, M., "Infrared focal plane arrays: state of the art and development trends", Proc. SPIE, Vol. 5126, 17th International Conference on Photoelectronics and Night Vision Devices, September, 2003.
14. Jensen, N., Optical and Photographic Reconnaissance Systems, John Wiley & Sons, Inc., New York, 1968.
15. Zhang, W., Ning, Y., Cao, Y., Zhang, X., "Lucky region imaging based on front and back defocus images comparison", Vol. 9796, Selected Papers of the Photoelectronic Technology Committee Conferences held November 2015, ,2016.
16. Castleman, K., Digital Image Processing, Prentice-Hall, New Jersey, 1996.
17. Simske, S., Dalong, L., "Atmospheric Turbulence Degraded-Image Restoration by Kurtosis Minimization", IEEE, Vol. 6, , 2009.
18. Laikin, M., Lens Design, Taylor-Francis CRC Press, FL, 2006.
19. Brosens, P., "Scanning speed and accuracy of moving magnet optical scanners", Optical Engineering, Vol. 34, No. 1, January, 1995.
20. Horn, S., "Cryogenic Cooling Options for Forward Looking Infrared (FLIR)", Proc. SPIE, Vol. 0245, Cryogenically Cooled Sensor Technology, November, 1980.
21. Chellis, F., "An Introduction to Closed Cycle Cryogenic Coolers", Proc. SPIE, Vol. 0245, Cryogenically Cooled Sensor Technology, November, 1980.

22. Li, X., Blinka, E., "Very Large FFT for TMS320C6678 Processors", Texas Instruments Inc., White Paper, 2015.
23. Pohl, K., Requirements Engineering Fundamentals, Principles, and Techniques, Springer-Verlag, Berlin-Heidelderg, 2010.
24. MIL-STD-1472F, Human Engineering, US Department of Defense, 1999.
25. MIL-STD-781C, Reliability Design Qualification and Production Acceptance Tests: Exponential Distribution, US Department of Defense, 1977.
26. MIL-HDBK-217, Reliability Prediction of Electrical Equipment, US Department of Defense, 1991.

Biography

John Hall

Mr. Hall works for the US Army DEVCOM C5ISR. He holds a BS Optics from the University of Rochester and an MS Electrical Engineering from George Mason University.

Steven Simske

Dr. Simske is a Professor of Systems Engineering at Colorado State University. Before joining CSU, Dr. Simske was at a NASA Center for the Commercial Development of Space (1990-1994, part-time till 2007) and at HP from 1994-2018, where he was an HP Fellow, Vice President, and Director in HP Labs.